PILATUS3 CdTe Detector Technology and its Applications

Tilman Donath, Ph.D., DECTRIS Ltd.
tilman.donath@dectris.com

Sections 1-4 of this whitepaper describe PILATUS3 CdTe detectors, which are the largest commercially available CdTe detectors for high-energy X-ray detection. Examples of these detectors' most typical applications are presented in the Appendix.

1. Introduction

In 2015, DECTRIS introduced the PILATUS3 CdTe detector family. With this new model, experiments using high-energy X-rays in the range of about 20 – 100 keV can benefit from the same Hybrid Photon Counting (HPC) detector technology that has transformed lower-energy X-ray research ever since the introduction of the PILATUS detectors in 2006. PILATUS3 CdTe detectors offer the same unique advantages: noise-free detection, a high dynamic range, sharp signals, and extremely high frame rates [1-3]. They are available both for the synchrotron (PILATUS3 X CdTe series) and for the laboratory (PILATUS3 R CdTe series). In this paper, we will focus on the detectors' applications at synchrotron beamlines.

PILATUS3 X CdTe detectors overcome the limitations of image plate, CCD, and flat-panel detectors, which are the typical „workhorse detectors" at high-energy beamlines (see the comparison of available high-energy detectors in Chapter 4 of both [4] and [5]). They are also much more sensitive to high-energy X-rays, even those above 50 keV, and can record weak signals without beeing impeded by readout noise or dark current. Frame rates of up to 500 Hz enable measurements to be made much more quickly, and measurements can also be performed continuously and without a shutter. Thanks to these features, the HPC detectors dramatically enhance a beamline's capabilities, making time-resolved, scanning, *in-situ* or *operando* experiments possible (see Figure 1 for an example).

As of early 2020, more than 15 large-area PILATUS3 CdTe systems are in use at synchrotron beamlines worldwide, including at APS, DLS, ESRF, PETRA III, PLS-II, SOLEIL, and SPring-8. More detectors will be installed later in 2020, including at SSRF and MAX-IV.

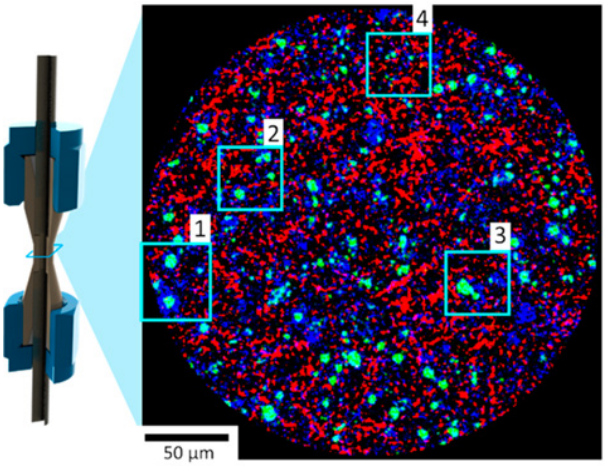


Figure 1: An operando study of a Li-ion microcell using XRD-CT at 50 keV (see the example of Finegan et al. in Appendix A.2).

2. Technical description and specifications

PILATUS3 CdTe detectors are built on the same platform as the highly successful PILATUS3 detectors and use the same PILATUS3 readout chip [6]. They all share a maximum achievable photon count rate of 10^7 photons·s^{-1}·pixel^{-1} ($3.4 \cdot 10^8$ photons·s^{-1}·mm^{-2}) and are fitted with CdTe sensors to achieve the best possible quantum

White Paper

Published online on 27 February 2020

Keywords: high energy, cadmium telluride, X-ray detector, hybrid photon counting, synchrotron radiation, scientific applications

DECTRIS
detecting the future

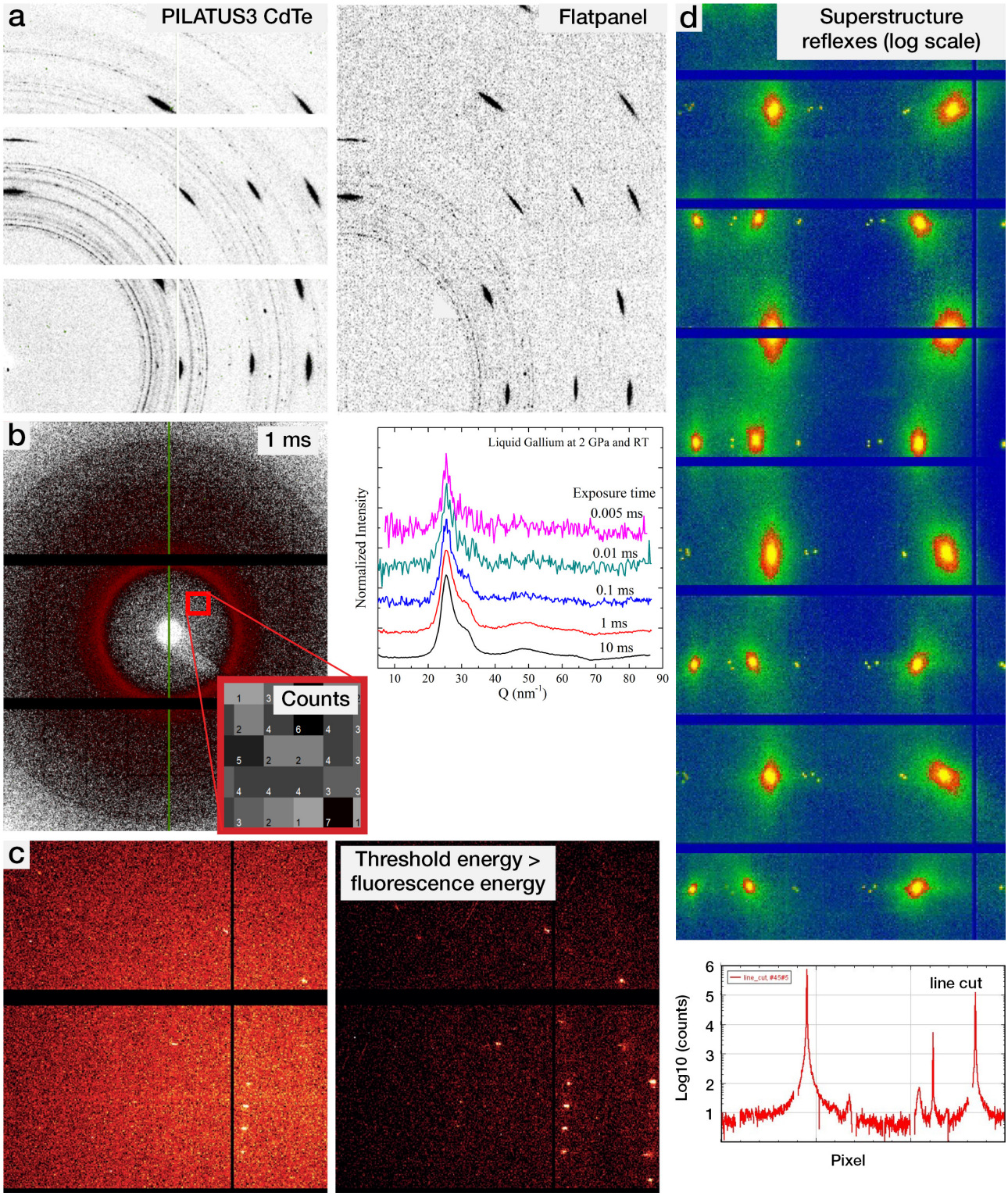


Figure 2: Example measurements that were obtained using PILATUS3 CdTe detectors. ***a)*** *A noise-free readout results in a high signal quality compared to that of a flat-panel detector and allows diffraction rings to be detected to a higher q value.* ***b)*** *Short exposure times allow for fast acquisition, or even time-resolved measurements, thanks to photon counting (the inset shows the photon counts for a subregion of pixels).* ***c)*** *Suppression of background from sample fluorescence when performing for quantitative analysis of weak signals is achieved by raising the threshold energy to be higher than the fluorescence energy.* ***d)*** *The high dynamic range of over 1:1,000,000 makes the signal between the diffraction spots visible.*
For experimental details and acknowledgments regarding these examples, see the footnote[1] at the end of the document.

White Paper

DECTRIS
detecting the future

efficiency over a wide energy range. Their energy threshold fully discriminates any electronic noise and can be employed to suppress sample fluorescence that creates detrimental background to the measurement.

For this purpose, the user can adjust the energy threshold up to 40 keV. Owing to the direct-conversion sensor, the pixel size of 172 µm determines the detector's spatial resolution, with a point-spread function that is only 1 pixel wide and results in optimal signal sharpness. In contrast to the light-emitting screen in scintillator-based detectors, the direct-conversion sensor is free of afterglow.
The performance characteristics of PILATUS3 CdTe detectors have been summarized in more detail in a previous publication [7]. These detectors' fundamental advantages are further demonstrated by the example measurements shown in Figure 2.

2.1 Quantum efficiency

While silicon offers efficient detection for energies between about 2 and 20 keV, the greater X-ray stopping power of a 1 mm thick CdTe sensor extends the range for X-ray detection up to about 100 keV, with high quantum efficiency (QE) over the entire photon energy range (Figure 3). The QE is above 90% up to the cadmium K edge at 26.7 keV, and stays above 80% up to approximately 80 keV.

2.2 A modular system architecture

The active surface of PILATUS3 CdTe detectors consists of an array of modules. Each module is about about 84x34 mm² in size and carries around 100,000 pixels. This modular system architecture is compatible with different rectangular detector sizes, ranging from ~100k to ~6M pixels, and also allows for customized detector shapes; see Figure 6 for an example. Each module comprises two CdTe sensor tiles with only a 1-pixel gap between them. The CdTe tiles with a size of 42 x 34 mm², as used in PILATUS3 detectors, are amoung the largest monolithic CdTe sensors available today.

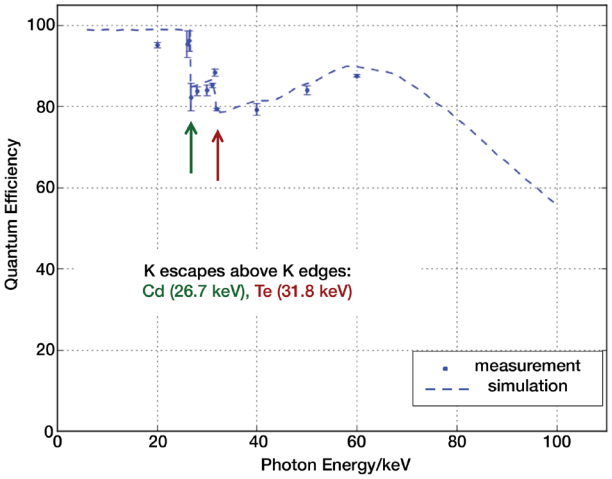


*Figure 3: The Quantum Efficiency (QE) of a PILATUS3 CdTe detector, measured from 20 to 60 keV with PTB at the BAMline at **BESSY II**. The threshold was set at 50% of the photon energy for each data point, and the measured QE follows the simulation **(the dashed line).** The reemission of fluorescence photons (called „escapes") causes the dips in QE that occur above the K absorption edges of cadmium **(the green arrow)** and tellurium **(the red arrow)**.*

2.3 Readout performance & system control

The PILATUS3 X CdTe series offers frame rates of up to 500 frames per second (fps) for full-frame readout; this applies to all detectors up to the 1M size (~1 million pixels). The 2M detector achieves 250 fps for full-frame readout and 500 fps for readout of a predefined region of interest (ROI), which can be up to eight modules (~800k pixels) in size. ROI readout modes are available on all PILATUS3 X 1M, 2M, and 6M detectors [8]. The readout time (dead time) of PILATUS3 X detectors is 0.95 ms.

The established readout & control interface of other PILATUS3 detectors ('camserver') is also used in all CdTe models, which makes detector integration and control straightforward.

The electronic gating (electronic shuttering) of PILATUS3 detectors enables time-resolved measurements to be made with exposure times down to or below 100 ns. Flexible internal or external triggering allows the detector to be synchronized with other experimental hardware: for example, with an external electric field and electronic delay in pump-probe-type measurements, or even with individual

White Paper

bunches of the pulsed synchrotron source (cf. [1]).

2.4 Stability, the polarization effect, and radiation hardness

For their sensor material, HPC detectors use mono-crystalline semiconductors, in which incoming X-rays are converted directly into electron-hole pairs. While Si excels with a virtually perfect crystal quality, lattice defects and impurities in CdTe crystals may cause trapping of the charge carriers. This can give rise to distortions in the electric field profile within the sensor, through a non-permanent effect known as polarization. Polarization can show up in the recorded images along preferred paths of the CdTe crystal, sometimes referred to as a network of lines. This effect, however, can be compensated with a flat-field image correction. Optimal sensor operating conditions (bias voltage and temperature), as implemented in the PILATUS3 series, allow polarization effects to be mitigated. Even under strong irradiation, the total signal recorded by PILATUS3 CdTe detectors is extremely stable, as was verified by a test at the BESSY-II synchrotron. The measurement from that test (Figure 4) shows a >1% variation of the total count signal over the entire 15-hour test. The readout chip of PILATUS3 detectors was designed to be radiation-hard. In detectors that are operated within their count-rate specification, permanent radiation damage has not been observed. Extreme overexposure, however, with photon rates many times above the detector's count-rate limit, can cause permanent damage to the readout chip and must be avoided; typically, only very intense direct synchrotron beams pose a risk in this regard. Fortunately, and in contrast to other detectors, radiation damage to a PILATUS3 detector typically stays confined to the overdosed pixels, leaving other pixels and modules unaffected.

3. Scientific applications

PILATUS3 CdTe detectors are used successfully in many fields which involve high-energy X-ray research. In Appendix A and Appendix B, we will present a few selected sample applications with references. Appendix A, „Materials & geological science," will present examples from X-ray powder diffraction (A.1.); diffraction tomography (A.2); total scattering for pair-distribution function (PDF) analysis (A.3); extreme-conditions experiments (A.4); and measurements "between the peaks" in inelastic and diffuse scattering, as well as in surface diffraction for measuring crystal truncation rods (A.5). Appendix B, „Crystallography," will present examples from high-energy crystallography, which are aimed at reducing radiation damage in macromolecular crystallography (B.1) and high-resolution data for charge density studies (B.2).

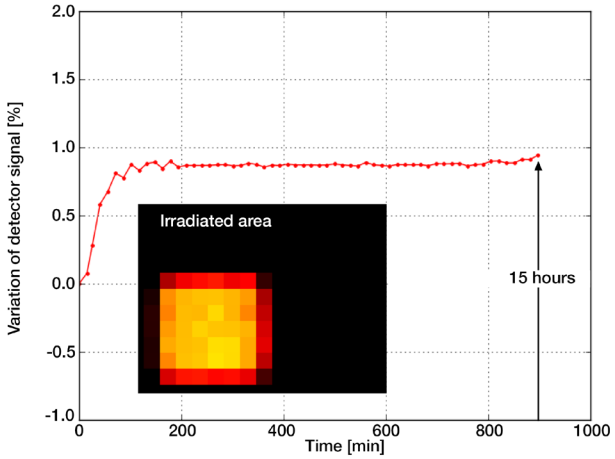


Figure 4: This graph shows the long-term stability of a PILATUS3 CdTe detector signal at high flux irradiation. Over 15 hours, the observed variation (relative change) of the total measured intensity signal was less than 1%. The inset shows an illuminated area approx. 5x5 pixels in size. The measurement was taken at 33 keV photon energy, with a count rate of ~2.5 x 10^6 photons/s/pixel (~8.5x10^7 photons/s/mm^2), at the BAMline at BESSY II, with the detector's signal normalized to the storage ring current.

4. Conclusions

PILATUS3 CdTe Hybrid Photon Counting detectors open up new experimental possibilities for high-energy X-ray research. Many high-profile publications are based on PILATUS3 CdTe data and attest to the detector's success. Despite minor deficiencies due to non-perfect CdTe crystals (compared to silicon crystals), PILATUS3 CdTe HPC detectors - thanks to their high speed and excellent data quality - enable researchers to make measurements that were impossible using image plate and scintillator-based detectors.

White Paper

DECTRIS
detecting the future

Appendix: Applications & references

A: Materials & geological science

In materials and geological science applications, the use of high-energy X-rays enables optimal penetration of the sample and its container, e.g. the powder capillary, or of the sample chamber in *in-situ* or *operando* measurements. The diffraction angles shrink with increasing energy, which gives researchers access to a wider q-range. On a large-area detector, it thus becomes possible to record the entire diffraction pattern in a single exposure. With the efficient PILATUS3 CdTe detector and the high flux that is available at modern high-energy synchrotron beamlines, high-quality (powder) diffraction patterns can be recorded within seconds or even milliseconds. The detector's high dynamic range eliminates the need for two separate exposures at a low dose and a high dose. Moreover, the absence of detector noise and the high stability of HPC detectors facilitate background subtraction when data measured without the sample in the X-ray beam need to be subtracted from the sample data.

A.1. Powder X-ray diffraction

In high-energy powder X-ray diffraction (PXRD), the noise-free readout and high dynamic range of PILATUS3 CdTe detectors permit signals to be recorded out to high diffraction angles and enable the detection of even weakly scattering components (dilute, amorphous, or nano-crystalline phases). This is true even if the components are in a mixture with well-diffracting crystalline phases (compare the example in Figure 2 a).

Schultheiss *et al.* [9] performed time-resolved *in-situ* PXRD to study the switching mechanism in polycrystalline ferroelectric/ferroelastic materials. At the ESRF ID15 beamline, using a PILATUS3 X CdTe 2M detector at its full frame rate of 250 Hz, they obtained 4-ms exposures that were of a high enough quality to allow the peak widths and positions to be analyzed with the accuracy that is necessary to characterize lattice strain. Thus, the entire irreversible polarization process could be studied in 10 seconds by recording 2,500 full powder patterns.

Liu *et al.* studied frequency-dependent decoupling of domain-wall motion and lattice strain in bismuth ferrite [10]. With an oscillating electric field applied to the sample, XRD patterns were acquired and time-resolved over the electric field cycle with 20 data points per cycle (see Figure 2 in [10]) and at electric field frequencies of up to 1,000 Hz, which require time resolution as low as 50 µs. To do this, a PILATUS3 X CdTe 2M detector was triggered in synchrony with the electric field oscillation and varying time delays. The detector's multiple-exposure feature was then used to sum up to 2,000 exposures internally and obtain the required statistics for the diffraction patterns before image readout took place. The images were then converted into one-dimensional diffraction patterns for subsequent peak fitting.

Lukin *et al.* used the PILATUS3 X CdTe 2M detector at the ESRF ID31 beamline to monitor mechano-chemical reactions inside a ball mill allowing for simultaneous XRPD and Raman scattering ([11]; see also DECTRIS News online [12]). Their real-time *in-situ* powder diffraction study revealed hitherto unknown phases and phase transformations in the mechanochemical reaction between benzoic acid and nicotinamide.

Dejoie *et al.* demonstrated the advantages of using a CdTe area detector in combination with a multi-crystal analyzer for fast scanning high-resolution PXRD measurements [13]. They used a single PILATUS3 X 300K-W detector to replace several 0D scintillation counters.

A.2 Diffraction tomography (XRD-CT, PDF-CT)

X-ray diffraction computed tomography (XRD CT) provides virtual powder diffraction data for each pixel in a tomographically reconstructed slice of the sample, thereby giving access to chemical information for each pixel. The method requires recording a huge number of powder diffraction patterns, while the sample is both rotated and laterally scanned through a pencil beam at each rotational step. In the example shown in

Figure 5, 13,000 diffraction patterns were acquired per scan.

The implementation of efficient XRD-CT acquisition schemes through the PILATUS3 X CdTe 2M detectors at ESRF beamlines ID15 and ID31 has accelerated the scanning process significantly. Today, time- and chemically-resolved studies are possible: for example, of catalytic reactions inside fuel cells or reactors, or of spatio-chemical processes inside batteries under *operando* conditions. The HPC detector enables higher scanning speeds for XRD-CT because it is noise-free and thus achieves sufficient signal-to-noise levels more quickly than older technology does. Even at high scanning speeds, the spatial resolution of an XRD-CT scan does not degrade due to the absence of afterglow, which would blur the signal in space during fast scans. Therefore, fine details - e.g. the emergence of the thin BaWO4 layer in Figure 5 - can be detected quantitatively.

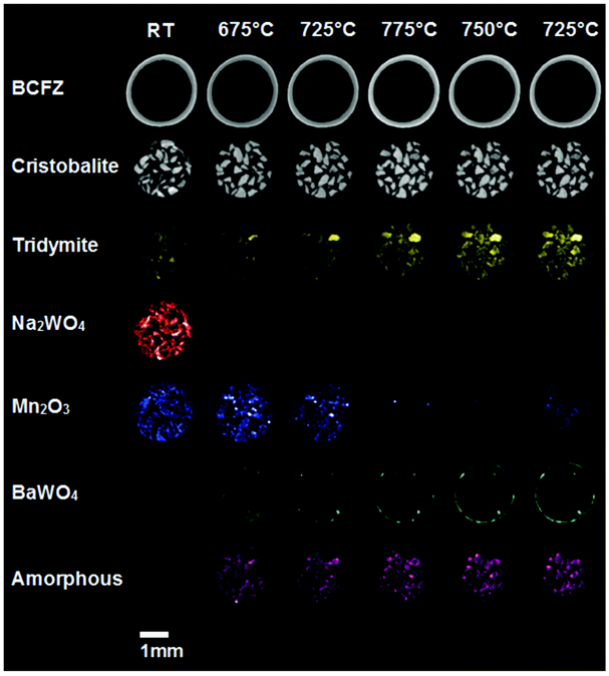


Figure 5 (Figure 2 from Vamvakeros et al. [14]): Diffraction CT results show the evolution of solid-state chemistry during a catalytic reaction as it takes place inside a catalytic membrane reactor. Phase maps for the relevant constituents ***(top to bottom)*** *were reconstructed from six XRD-CT scans, which were performed as a function of temperature/time* ***(left to right).*** *The measurements were taken at ESRF ID15 with a beam of 93 keV, focused to 20x20 μm². 130 projections × 100 translations (13,000 total diffraction patterns) were acquired per scan using a PILATUS3 X CdTe 300K detector prototype in 2014.*

In 2018, Vamvakeros *et al.* presented time-resolved and *operando* XRD-CT measurements of acatalyst bed which were recorded at ESRF ID31 within 108 seconds [15]. Their article includes a review of XRD-CT's development and applications; it also compares the speed of measurements published between 2008 and 2016 (Suppl. Table 4 in Suppl. Note 2 of [15]). Remarkably, the acquisition time per scan point decreased from 10 seconds in 2008 to 15 ms in the scans from the study ten years later. Correspondingly, the scan time per slice was reduced by more than two orders of magnitude for the same spatial resolution. This enables enhanced time resolution, or the ability to record multiple 2D slices or an entire 3D volume of the sample, as demonstrated in the study.

The faster scanning capability of PILATUS3 X CdTe detectors also allows for increased spatial resolution. Recently, Finegan *et al.* presented a study on the lithiation of Li-ion electrodes, which used a combination of high-speed XRD at up to 100 fps and high-resolution XRD-CT [16]. Both measurements were taken using the PILATUS3 X CdTe 2M detector at the ESRF beamline ID 15A, with a 50-keV beam focused to 1 μm. The high-resolution XRD-CT scans included ROI scans with 301 lateral scan points for 300 rotation steps (90'100 diffraction patterns). Figure 1 shows a high-resolution phase map of three relevant phases inside the Si-graphite electrode, shown as a multicolor image (a reproduction of Figure 5a from [16]).

A.3 Total scattering for pair-distribution-function (PDF) analysis

PDF analysis with high, real-space resolution requires collecting data at high values of q with accurate intensities and high counting statistics. However, at high X-ray energies and high q values, a large part of the signal consists of Compton scattering, which carries no useful structural information. And so, this and other corrections to the observed intensity have to be carried out analytically or semi-empirically. A photon-counting detector helps in the analysis, thanks to its accurate intensities. Moreover, subtracting the scattering

background or the PDF signal of another sample (difference PDF, cf. Section 2.5) introduces fewer artifacts than it did in the past.

Best *et al.* carried out 1D-scanning PDF measurements on 3D-printed bulk metallic glass (which had been produced by means of laser-additive manufacturing). The data were acquired in transmission using 98.15-keV photon energy and the PILATUS3 X CdTe 2M-PETRA III detector at PETRA III's P07 beamline at the Deutsches Elektronen-Synchrotron (DESY) [17]. Scanning with a step size of 2 µm, while recording almost 5,000 diffraction patterns per sample, revealed periodic changes in the pair distribution function which could be explained by a local strain variation of only +/-0.1%. According to beamline scientist and coauthor Ann-Christin Dippel, the CdTe detector, being free of afterglow, was essential for detecting these minute changes in the diffraction signal while fast-scanning over the samples.

Luo *et al.* performed a PDF experiment on ultra-thin (2-20 µm) metallic glass samples, which give only a feeble diffraction signal at the applied beam energy of 79.5 keV [18]. By placing the PILATUS3 X CdTe 2M detector off-center and close to the sample, the authors accessed reciprocal space up to ~30 $Å^{-1}$. The noise- and background-free HPC detector helped them to achieve the high data quality that the study required (compare Figures 2b and 3a in [18]).

Further PDF studies based on PILATUS3 X CdTe data have also been published: by Pathak *et al.* [19] on super-cooled water in a droplet train; by Ferri *et al.* [20] on heavy metal trapping on the surface of hydroxyapatite; and by Poulain *et al.* [21] on a study of pyrolyzed wood, which combined WAXS and PDF analysis. Data processing for PDF analysis, especially focused on parallax correction, has been described by Marlton *et al.* [22].

A.4 Extreme conditions (High-pressure and high-temperature studies)

In high-pressure studies inside a diamond anvil cell (DAC), an elevated photon energy ensures efficient penetration of the several-millimeter-thick diamond anvils, as well as sufficient q-range coverage through the high-pressure device's limited angular opening. Therefore, the high efficiency of PILATUS3 X CdTe detectors presents a big advantage for DAC experiments, compared to what is offered by previous detector technologies. In a recent review, Shen and Mao describe how advanced types of DAC measurements (rapid compression and decompression, modulated laser heating, and equation of state studies) benefit from the time resolution, gating capability, and fast framing of photon-counting detectors ([23]; see Sections 2.6, 2.7.5, and 4.2, respectively.

Drozdov *et al.* reported superconductivity in lanthanum hydride under high pressures of 170 gigapascals with a high critical temperature of 250 K [24]. Using the PILATUS3 X CdTe 1M detector at APS beamline 13-ID-D, they obtained PXRD measurements at around 40 keV with a beam size of ~3×4 $µm^2$, by 2D-scanning the sample through the beam inside a DAC. According to coauthor Eran Greenberg (postdoc at GSECARS, University of Chicago), the PILATUS3 CdTe detector's fast framing capability and high data quality were essential in this study. These characteristics enabled fast 2D scanning of the sample with a small X-ray spot, which allowed the team to quickly identify which phases on the sample were the superconducting ones.

The ID06 Large Volume Press (LVP) beamline at the ESRF recently installed a customized PILATUS3 X CdTe 900K-W detector (Figure 6) with nine horizontally arranged modules. With its wide active area of 763.5 x 33.5 mm^2 and high resolution of 4439 x 195 pixels, the detector will cover the wide angular range accessible through the LVP.



Figure 6: This customized PILATUS3 X CdTe 900K-W-ESRF detector was designed for the ID06 Large Volume Press beamline at ESRF.

White Paper

A.5 Between the peaks: Inelastic scattering, diffuse scattering, and surface diffraction

Studies using inelastic scattering, diffuse scattering, or surface diffraction (crystal truncation rods) from crystals depend on the diffraction signal between the Bragg peaks, which is typically several orders of magnitude weaker than the diffraction spots. CdTe-based HPC detectors enable the recording of weak signals, even when those signals are close to strong peaks. Thanks to the detector's high dynamic range of 1:1,000,000, Bragg peaks may be measured quantitatively at the same time as the inelastic and diffuse signals.

Krogstad *et al.* studied ionic correlations of intercalation compounds that are relevant to the performance of batteries [25]. The 3D-ΔPDF method that they applied extends PDF analysis to access the deviation of crystalline samples from perfect single crystals, based on the measurement of the diffuse scattering signal. The data were obtained using a PILATUS3 X CdTe 2M detector at APS beamline 6-ID-D, using X-rays of 87.1 keV. With the introduction of the CdTe detectors, it is now possible to measure sufficiently complete 3D volumes of reciprocal space in under 20 minutes, which makes the generation of robust ΔPDFs fast enough to allow detailed studies as a function of temperature. The data correction methods that the authors applied are described in the supplement to their article.

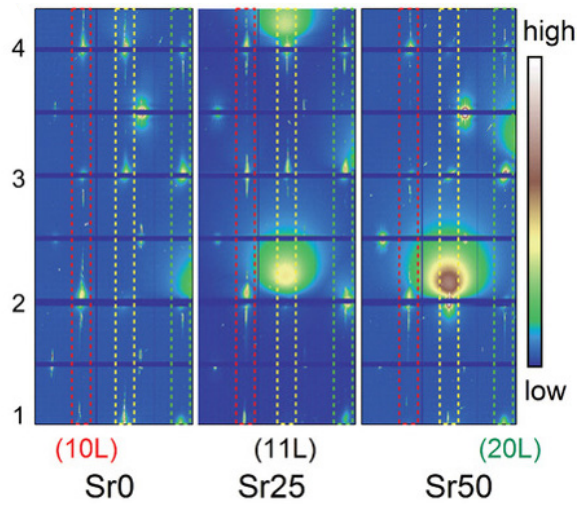


Figure 7 (Figure 1c from [26]): These reciprocal space maps for the crystal truncation rods of LSNO thin films were recorded using a PILATUS3 X CdTe 2M detector. (The broad spots arise from parasitic scattering of tungsten stripes that are used to block the extremely strong Bragg peaks from the substrate.)

Liu *et al.* applied high-energy X-ray surface diffraction (crystal truncation rod measurements) to study thin films of the oxygen electrocatalyst $La_{1-x}Sr_xNiO_3$ [26]. Epitaxial thin film samples of the catalyst, grown on a single-crystal substrate, were measured at 85 keV at the APS beamline 1-ID. The PILATUS3 CdTe 2M detector's large area and high quantum efficiency enabled large 3D reciprocal space volumes to be captured rapidly (Figure 7).

More "between-the-peaks" data that have been collected using PILATUS3 CdTe detectors include: the measurement of crystal truncation rods of thin films in transmission and *operando* by Reikowski *et al.* [27]; and inelastic scattering measurements of highly absorbing bismuth crystals at 79.6 keV presented in [28] by Minelli *et al.*

B: Crystallography

B.1 Macromolecular crystallography (MX)

Macromolecular crystallography (MX) at elevated X-ray energies of ~30 keV holds the potential for an increased signal-per-unit dose, equivalent to less radiation damage at a given resolution ([29], [30]; see also DECTRIS News online [31]). CdTe-based HPC detectors, which offer the same advantages regarding sensitivity and data quality as their silicon-based cousins at typically employed energies (5-15 keV), make it feasible to exploit the expected benefits for MX at high energies. To maximize the positive effects, data should be collected below the absorption edge of cadmium (26.7 keV).

In 2019, Takaba *et al.* published a charge density analysis of the chromophore of green fluorescent protein (GFP), with diffraction data obtained to a resolution better than 0.8 Å at photon energy of 35.4 keV [32]. In addition, Ueno *et al.* determined the low-dose structure of the radiation-sensitive metal protein cytochrome C oxidase (CcO) in its resting oxidized state at 30 keV photon energy [33]. Exposed to only 58 kGy of radiation, the bond length between the peroxide ligand and CcO was comparable to that determined from data that

had been obtained at an X-ray free-electron laser, and thus were largely free of radiation damage. The data for both studies were collected using a PILATUS3 X CdTe 300K detector at SPring-8 beamline BL41XU.

B.2 Charge density studies

Charge density studies require data of the highest resolution and accuracy in order to analyze differences between the experimental electron density and that which can be calculated from a model. High-resolution data can be acquired more efficiently at high X-ray energies, where diffraction angles are compressed. Hence, for charge density investigations at synchrotrons, the specifications of PILATUS3 X CdTe detectors were quickly recognized as promising, mainly due to the detectors' high detection efficiency in the high-energy X-ray regime and their high dynamic range and low noise. These characteristics should overcome the perpetual problem of detecting strong and weak reflections simultaneously [34].

Charge density studies also require the highest resolution in order to refine deviations from the spherical atom model. A large number of reflections is thus required, and the recorded data need to be accurate. Charge density measurements were recently taken using the PILATUS3 X CdTe 1M detector at the BL02B1 beamline of the SPring-8 synchrotron in 2018. These measurements show that high-quality single-crystal data can be obtained with a CdTe detector ([34], *results soon to be published*).

Finally, Figure 1c of this white paper shows images demonstrating fluorescence suppression using a PILATUS3 R CdTe 300K detector in the laboratory for a small-molecule study.

References

1. A. Miceli, *J. Instrum.* **4**, P03024 (2009), doi:10.1088/1748-0221/4/03/P03024.

2. C. Brönnimann *et al.*, in *Synchrotron Light Sources and Free-Electron Lasers*, E. Jaeschke et al., Eds. (Springer International Publishing, Cham, 2018, pp. 1–33). doi: 10.1007/978-3-319-04507-8.

3. A. Förster *et al.*, *Philos. Trans. R. Soc. Math. Phys. Eng. Sci.* **377**, 20180241 (2019), doi:10.1098/rsta.2018.0241.

4. U. Lienert et al., "PETRA III Extension Project - Beamline P21 Swedish High Energy Materials Science Beamline - Technical Design Report" (2013). Available online, accessed on 18 February 2020.

5. B. B. He, *Two-dimensional X-ray Diffraction, Second Edition* (John Wiley & Sons, Ltd, 2018). doi: 10.1002/9781119356080.

6. T. Loeliger et al., in *2012 IEEE Nuclear Science Symposium and Medical Imaging Conference Record (NSS/MIC)* (2012), pp. 610–615. doi: 10.1109/NSSMIC.2012.6551180.

7. D. Šišak Jung *et al.*, *Powder Diffr.* **32**, S22–S27 (2017), doi:10.1017/S0885715617001191.

8. "ROI_add_on-PILATUS3_X_V2.pdf," a document describing region-of-interest readout in PILATUS3 X 1M, 2M and 6M detectors, available online.

9. J. Schultheiß *et al.*, *Acta Mater.* **157**, 355–363 (2018), doi:10.1016/j.actamat.2018.07.018.

10. L. Liu *et al.*, *Nat. Commun.* **9**, 4928 (2018), doi:10.1038/s41467-018-07363-y.

11. S. Lukin *et al.*, *Chem. – Eur. J.* **23**, 13941–13949 (2017), doi:10.1002/chem.201702489.

12. DECTRIS News article "Featured laboratory: Laboratory for Green Synthesis at the Ruder Boškovic Institute"; published online on 13. August 2019.

13. C. Dejoie *et al.*, *J. Appl. Crystallogr.* **51**, 1721–1733 (2018), doi:10.1107/S1600576718014589.

14. A. Vamvakeros *et al.*, *Chem. Commun.* 51, 12752–12755 (2015), doi:10.1039/C5CC03208C. *Figure 5 above is reproduced from Figure 2 in this article, which was published by the Royal Society of Chemistry and licensed under a Creative Commons Attribution 3.0 Unported Licensce.*

15. A. Vamvakeros *et al.*, *Nat. Commun.* **9**, 4751 (2018), doi:10.1038/s41467-018-07046-8.

16. D. P. Finegan *et al.*, *Nano Lett.* **19**, 3811–3820 (2019), doi:10.1021/acs.nanolett.9b00955. *Figure 1 above is reprinted (adapted) with permission from Figure 5 in the article. ©2019 American Chemical Society.*

White Paper

DECTRIS
detecting the future

17. J. P. Best *et al.*, *Appl. Phys. Lett.* **115**, 031902 (2019), doi:10.1063/1.5100050.

18. P. Luo *et al.*, *Nat. Commun.* **9**, 1389 (2018), doi:10.1038/s41467-018-03656-4.

19. H. Pathak *et al.*, *J. Chem. Phys.* **150**, 224506 (2019), doi:10.1063/1.5100811.

20. M. Ferri *et al.*, *Appl. Surf. Sci.* **475**, 397–409 (2019), doi:10.1016/j.apsusc.2018.12.264.

21. A. Poulain *et al.*, *J. Appl. Crystallogr.* **52**, 60–71 (2019), doi:10.1107/S1600576718017685.

22. F. Marlton *et al.*, *J. Appl. Crystallogr.* **52**, 1072–1076 (2019), doi:10.1107/S1600576719011580.

23. G. Shen *et al.*, *Rep. Prog. Phys.* **80**, 016101 (2017), doi:10.1088/1361-6633/80/1/016101.

24. A. P. Drozdov *et al.*, Nature. **569**, 528–531 (2019), doi:10.1038/s41586-019-1201-8.

25. M. J. Krogstad *et al.*, *Nat. Mater.*, 1–6 (2019), doi:10.1038/s41563-019-0500-7.

26. J. Liu *et al.*, *Adv. Sci.* **6**, 1901073 (2019), doi:10.1002/advs.201901073. *Figure 7 above is reproduced from Figure 1c in the article, which is published under an Attribution 4.0 International (CC BY 4.0) license.*

27. F. Reikowski *et al.*, *J. Phys. Chem. Lett.* **8**, 1067–1071 (2017), doi:10.1021/acs.jpclett.7b00332.

28. A. Minelli *et al.*, *Phys. Rev. B.* **100**, 104305 (2019), doi:10.1103/PhysRevB.100.104305.

29. J. L. Dickerson *et al.*, *J. Synchrotron Radiat.* **26**, 922–930 (2019), doi:10.1107/S160057751900612X.

30. A. Förster *et al.*, *Struct. Dyn.* **6**, 064302 (2019), doi:10.1063/1.5131017.

31. DECTRIS News article "More data, less damage," published online on 5 November 2019.

32. K. Takaba *et al.*, *IUCrJ.* **6**, 387–400 (2019), doi:10.1107/S205225251900246X.

33. G. Ueno *et al.*, *J. Synchrotron Radiat.* **26**, 912–921 (2019), doi:10.1107/S1600577519006805.

34. L. Krause *et al.*, „Measuring accurate single crystal data using a PILATUS3 CdTe detector," 32nd European Crystallographic Meeting, abstract of presentation MS38-P04. Available online; accessed on 18 February 2020.

[1]Experimental details and acknowledgments for Figure 2: **(a)** Static powder diffraction patterns recorded at ESRF ID 15 at 46.3 keV comparing PILATUS3 CdTe 300K and beamline flatpanel at same solid angle (same flux) per pixel, same exposure time 100 ms. Sample: superconducting filament containing Nb_3Sn powder in a tungsten tube (Ø 50 µm). Relevant for the study were the powder rings, which could be clearly detected even with the presence of strong reflections from the tungsten tube (dark spots). Courtesy M. Di Michiel, G. Vaughan, ESRF ID15A; C. Scheuerlein, CERN. **(b)** Diffraction patterns of liquid Ga in diamond anvil cell at 2 GPa recorded at APS HPCAT using PILATUS3 X CdTe 300K at 30.5 keV. Courtesy: Stas Sinogeikin, Yue Meng, Changyong Park, HPCAT, APS. **(c)** Chemical crystallography on diphenyl selenide crystal demonstrating suppression of selenium fluorescence (Ka at 11.2 keV) by the detector's energy threshold, recorded with PILATUS3 R CdTe 300K in laboratory diffractometer using Ag radiation (22.2 keV). Courtesy Dietmar Stalke, Georg-August-Universität Göttingen. **(d)** Study of superstructure reflexes in a single crystal of the shape memory alloy NiFeCoGa at a photon energy of 106 keV using PILATUS3 X CdTe 2M detector of the APS detector pool. The image shows the sum of 60 exposures each acquired for 0.2 seconds during crystal rotation over 120°. Inset: line cut showing that 6 orders of signal amplitude can be resolved. Courtesy: Uta Rütt, APS at ANL.

White Paper

DECTRIS
detecting the future